Investigation of combinatorial coevaporated thin film Cu_2ZnSnS_4 (II): Beneficial cation arrangement in Cu-rich growth

E. A. Lund,[1] H. Du,[2,a)] W. M. Hlaing OO,[3] G. Teeter,[4] and M. A. Scarpulla[1,3,5,b)]
[1]*Department of Chemical Engineering, University of Utah, 50 S. Central Campus Dr. Rm 3290, Salt Lake City, Utah 84112, USA*
[2]*Sion Power Corporation, 2900 E Elvira Rd., Tucson, Arizona 86756, USA*
[3]*Department of Materials Science and Engineering, University of Utah, 122 S. Central Campus Dr. Rm 304, Salt Lake City, Utah 84112, USA*
[4]*National Renewable Energy Laboratory, 15013 Denver West Parkway, MS3218, Golden, Colorado 80401, USA*
[5]*Department of Electrical and Computer Engineering, University of Utah, 50 S. Central Campus Dr. Rm 3280, Salt Lake City, Utah 84112, USA*

(Received 7 November 2013; accepted 6 April 2014; published online 2 May 2014)

$Cu_2ZnSn(S,Se)_4$ (CZTSSe) is an earth-abundant semiconductor with potential for economical photovoltaic power generation at terawatt scales. In this work, we use Raman scattering to investigate phase coexistence in combinatorial CZTS thin films grown at 325 or 470 °C. The surface of the samples grown at 325 °C is rough except for a prominent specularly reflective band near and along the ZnS-Cu_2SnS_3 (CTS) tie line in the Cu-Zn-Sn-S quaternary phase diagram. All structurally incoherent secondary phases (SnS_2, CuS) exist only as surface phases or are embedded as separate grains, whereas the structurally coherent secondary phase CTS coexists with CZTS in the dense underlying film. In films grown at 325 °C, which are kinetically trapped by the low growth temperature, a change is observed in Cu and Sn site occupancy, evidenced by the shift from cubic-CTS in the Cu-rich region (Cu/Sn > 2) to more tetragonal-CTS in the Sn-rich region (Cu/Sn < 2). For CZTS samples grown at 470 °C, CTS is not observed and regions grown under excess Sn flux are more disordered than Cu-rich regions evidenced by broader CZTS A mode peaks. Therefore, increasing Sn chemical potential results in more CZTS lattice disorder, suggesting, with other evidence, the formation of Sn antisite defects. In contrast, the CZTS A mode breadth is insensitive to Zn richness suggesting that excess Zn does not induce significant disorder within the CZTS lattice. We postulate that initially growing CZTS films Cu-rich (Cu/Sn > 2) results in higher cation ordering meaning fewer antisite defects. © *2014 AIP Publishing LLC*.
[http://dx.doi.org/10.1063/1.4871665]

I. INTRODUCTION

$Cu_2ZnSn(S,Se)_4$ (CZTSSe), a semiconductor used as an absorber layer in thin film solar cells, poses an alternative to $Cu(In,Ga)Se_2$ (CIGSe) due to the constituent elements' relatively low costs and large industrial availability. Recent thin film solar cell device efficiencies of 12.6% (Ref. 1) for mixed sulfoselenide (CZTSSe) absorbers and 8.4% (Refs. 2 and 3) for the pure sulfide (CZTS) demonstrate the viability of this material for use in practical thin film technologies. However, the compositional region of thermodynamic stability for the pure CZTS phase is quite small on the bulk pseudo-ternary phase diagram at temperatures relevant for thin film synthesis,[4,5] which indicates the formation of secondary phases such as ZnS, Cu_xSnS_{x+1}, Sn_xS_y, and Cu_xS is probable with variations in stoichiometry.

The defects and secondary phases that result from compositional variation both positively and negatively affect CZTSSe devices. $Cu_{2-x}S(Se)$ phases in the final film may cause shunting due to both the high conductivity and contact with front and back CZTS(Se) interfaces. Nevertheless, it is also used as a fluxing agent to promote lateral grain growth during the initial stage of CZTSe (Ref. 6) coevaporation. ZnS phase separation from CZTS at the back interface lowers the open circuit voltage (V_{OC}) of a CZTS device[7] and ZnSe within the space-charge region of a CZTSe film blocks charge collection due to band structure misalignment with CZTSe.[8] Even though ZnS(Se) phase precipitation lowers CZTS(Se) device performance,[9,10] a final Zn-rich, Cu-poor film composition yields higher device V_{OC} and agrees with the prediction[11] that the defect complex $[V_{Cu}^{-} + Zn_{Cu}^{+}]^0$ formed in this compositional regime may maximize CZTS(Se) device performance. Secondary phases including ZnS and Cu_2SnS_3 (CTS) that have similar crystalline structures to CZTS may also passivate grain boundaries[12] by reducing strain and lowering recombination velocities at the grain interfaces. Although CTS may play a positive role in grain boundary passivation, its lower bandgap (0.8–0.9 eV for CTS and 0.4 eV for CTSe)[13] may decrease V_{OC} for CZTS devices and, therefore, reduce overall solar cell efficiency.

The current record efficiency kesterite device was made by a non-vacuum hydrazine processing method, whereas all record-efficiency CIGSe devices over the last 20 years[6] have

[a)]This work was performed while H. Du was at National Renewable Energy Laboratory, 15013 Denver West Parkway, MS3218, Golden, Colorado 80401, USA.
[b)]Author to whom correspondence should be addressed. Electronic mail: scarpulla@eng.utah.edu.

been deposited by coevaporation. An advantage of coevaporative growth is the tunability of composition through the film thickness, which can control the bandgap and phases present as well as maintain high overpressure of volatile species during long growth runs at high temperature. Nevertheless, coevaporative growth of CZTSSe is encumbered by the high substrate temperatures necessary for quality grain growth, which causes SnS loss and CZTS decomposition into binary $Cu_{2-x}S$ and ZnS.[14–16] Despite these challenges, a 9.15% efficient CZTSe device has been made using a 2-stage coevaporation process, which incorporates a transition from Cu- to Zn-rich growth.[6] Kaune *et al.*[17] demonstrate the conversion of $Cu_{2-x}Se$, SnSe, and ZnSe directly into CZTSe during the 2-stage coevaporation of CZTSe; however, CZTS(Se) grown at low temperature (<400 °C) develops an intermediate CTS(Se) phase, which requires higher temperature processing to convert to CZTS(Se).[18,19] These observations emphasize that both temperature and composition affect the phases which coexist with CZTS during growth.

For low-quality or small-grained films, the CTS and ZnS secondary phases are difficult to distinguish from CZTS by x-ray diffraction (XRD), which further complicates the development and evaluation of phase-pure CZTS films. Raman spectroscopy has been shown to resolve some secondary phases from CZTS, and both lateral and depth resolution at the scale of grains have been achieved.[20] Raman studies on CZTS published to date examined samples intended to be compositionally homogeneous across the films.

In this work, we examine compositionally graded, or "combinatorial," CZTS thin films to isolate the effects of composition on phase formation during growth. The samples are similar to those studied and characterized by Du *et al.*[21] in part 1 of this 2-part study. These unique films deposited by coevaporation of elemental Cu, Zn, Sn, and S sources in a molecular beam epitaxy system cover a wide stoichiometric range with all other variables constant.

For films deposited at 325 °C, there is a clearly visible specular band corresponding to the ZnS-CZTS-Cu_2SnS_3 tie line, which follows the ratio Cu/Sn ~ 2 in CZTS pseudo-ternary phase diagrams. The surface roughness on either side of the specular band is due to Cu_xS and Sn_xS_y surface phases. Both tetragonal- and cubic-Cu_2SnS_3 ($I\bar{4}2m$ tet- and $F\bar{4}3m$ cub-CTS) coexist with CZTS, even in Zn-rich regions where only ZnS and CZTS are expected. The CTS shifts from more cub- to more tet-CTS as the composition shifts from Cu-rich (Cu/Sn > 2) to Sn-rich (Cu/Sn < 2) and from Zn-poor (Cu/Zn > 2) to Zn-rich (Cu/Zn < 2). The change in CTS phase indicates that composition influences the Cu and Sn cation ordering in CTS.

As expected, films grown at 470 °C do not contain CTS and final CZTS crystalline quality is improved with increased growth temperature. The change in Cu and Sn cation ordering within the similarly zinc-blende based CTS phases observed at low growth temperature and the marked increase in CZTS crystalline quality when the high temperature growth sample shifts from Sn-rich to Cu-rich indicates Cu-rich growth may lead to less disorder within CZTS. Our findings are consistent with part 1 of this study, which found dramatically higher photoluminescence (PL) yields in Cu-rich versus Sn-rich regions of the films. The deleterious effects of excess Sn are attributed to native Sn-related defects, which we postulate can be minimized by initial Cu-rich growth. A larger Zn fraction in the sample has relatively little effect on the overall crystalline quality as analyzed by Raman spectroscopy.

II. MATERIALS AND METHODS

A. Deposition of combinatorial thin films

The CZTS films were deposited in a high vacuum physical vapor deposition system with either 325 or 476 °C substrate heating. Cu, Zn, and Sn were evaporated from effusion cells, and S was supplied through a valved cracker. The deposition chamber was equipped with translatable apertures that partially block the metal flux from each source to introduce a graded distribution of the specific element. No aperture was used for the sulfur source. The metal sources with combinatorial apertures were oriented 120° with respect to each other, resulting in films with metal spatial composition gradients. The *ex situ* calibration of the growth rate for this experiment was about 2.1 Å/s, and the films were approximately 0.75–1.5 μm thick. Substrates were molybdenum-coated soda lime glass (SLG/Mo) with dimensions 15 mm × 20 mm. This study encompasses 3 "low temperature" films grown at 325 °C and one "high temperature" film grown at 470 °C with excess fluxes of S and Sn to prevent CZTS decomposition. The three low temperature films have composition ranges containing a point corresponding to stoichiometric CZTS, a film with significant Zn excess, and another film with no Zn. The high temperature film had a small excess of Sn flux during cooling to prevent decomposition and formation of Cu_xS. A detailed description of the deposition is provided in part 1.[21]

B. Raman spectroscopy, scanning electron microscopy (SEM), and X-ray fluorescence (XRF)

Raman spectroscopy was done using an excitation wavelength of 488 nm in a WiTec AlfaSNOM confocal microscope system in the backscattering configuration. The instrument was equipped with a 10× magnification and 0.25 numerical aperture lens. The laser-illuminated spot on the samples was 20 μm in diameter, and the data were collected from a 2 μm area within that spot using the pinhole of the confocal system after carefully focusing each point at the surface of the film. A long-pass filter was employed, which has a cut-on wavelength of 492.8 nm. The absolute wavenumber calibration of the system was measured with a crystalline Si wafer before collection of each data set, and the laser power was adjusted sufficiently low to ensure that the CZTS peaks were not shifted by thermal effects. The metal and sulfur atomic percentages reported for each Raman analysis spot were determined using energy dispersive x-ray spectroscopy (EDS) in an FEI Quanta SEM at an accelerating voltage of 15 keV. The sampling area was 20 μm × 20 μm for the EDS analysis to avoid complications from local fluctuations as the Raman and EDS were measured in different instruments. The Raman signals changed

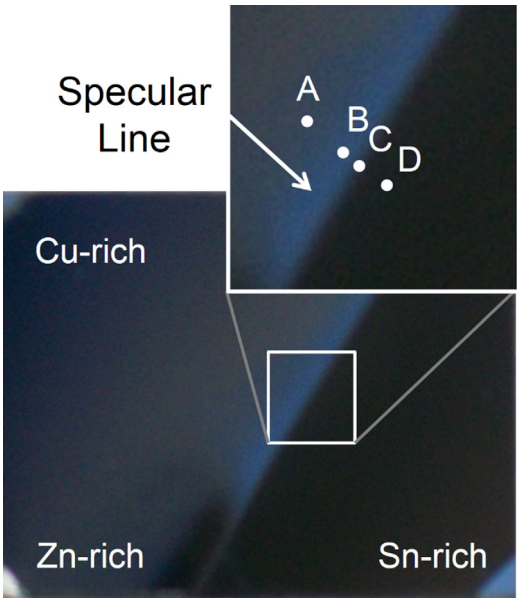

FIG. 1. Diffuse light image of a typical combi-CZTS sample grown at 325 °C showing the specular band. The corners of the sample closest to the respective metal effusion cell sources are labeled Cu-, Sn-, and Zn-rich. Analysis spot C lies just at the transition between specular and rough morphologies. Spots A-D all lie along a line perpendicular to the specular band (spacing not to scale). Spot B lies in the shiniest part of the specular band, 200 μm towards the Cu-rich region from the specular/rough edge. Spot A is 700 μm from spot C into the Cu-rich region. Spot D is 250 μm from point C but in the Sn-rich region.

sufficiently slowly with distance across the sample that the data presented for each analysis spot are representative of the area sampled by EDS. XRF measurements were also made of Cu, Zn, and Sn on a regular grid over the entire sample area with a mm-sized probe and were used to create the compositional contour plots.

III. RESULTS AND DISCUSSION

A. Low temperature films deposited at 325 °C

1. Surface morphology

The compositionally graded CZTS thin films deposited at 325 °C vary in surface morphology due to composition-dependent variation of secondary phases. The diffuse light image of a typical sample (Fig. 1) shows the most notable feature of these low temperature samples: a distinct specularly reflective band running diagonally across the film. Compositional contour maps (Fig. 2) of another combi-CZTS sample deposited under similar conditions demonstrate that the [Cu]/[Sn] ratio correlates with surface roughness on both sides of the specular band. As discussed in part 1,[21] the specular band appears in the region of the sample containing only CZTS and structurally coherent secondary phases including ZnS and cub- and tet-CTS.

The morphological transition from a rough surface to the smooth specular band is gradual on the Cu-rich side, whereas it is abrupt on the Sn-rich side. On the Cu-rich side, Cu_xS is present predominantly as ~1 μm crystals of CuS on top of the CZTS film with the areal density gradually decreasing towards and into the specular region. Part 1[21] shows that the Cu-rich region of a similar sample contains both surface and embedded CuS and Cu_2S crystals in a densely packed film. On the Sn-rich side of the film, the morphology abruptly changes from a very smooth, dense film with no surface phases on the specular band to a thin, porous film of densely packed CZTS with flake-like SnS_2 on top.[21] Part 1 presents XRD and SEM data with the discussion of the correlation of rough or smooth surface morphology to the secondary phases that are structurally incoherent (SnS_2 and Cu_xS) or structurally coherent (CTS and ZnS).

2. Composition

EDS compositional mapping of two low temperature samples, a "regular" and a "Zn-rich" sample, shows a wide variation in Zn composition (Fig. 3) along the specular band. The "Zn-rich" sample was deposited under the same conditions as the "regular" sample, except with a higher Zn flux. In the specular band, the Zn/(Cu + Sn + Zn) fraction spans Zn-poor (0.18) to Zn-rich (0.68) along the ZnS-Cu_2ZnSnS_4-Cu_2SnS_3 tie line of the CZTS quaternary phase diagram, indicating that compositions along this tie line result in lower densities of surface phases. Similar XRF compositional studies also agree with this finding.[21]

The phases detected by Raman spectroscopy in thin films grown at 325 °C include CZTS, SnS_2, Cu_2S, CuS, tet- and cub-CTS, and orthorhombic-Cu_3SnS_4. However, these phases are not all contained exclusively on either the CuS-ZnS-SnS pseudo-ternary phase diagram shown in Fig. 3

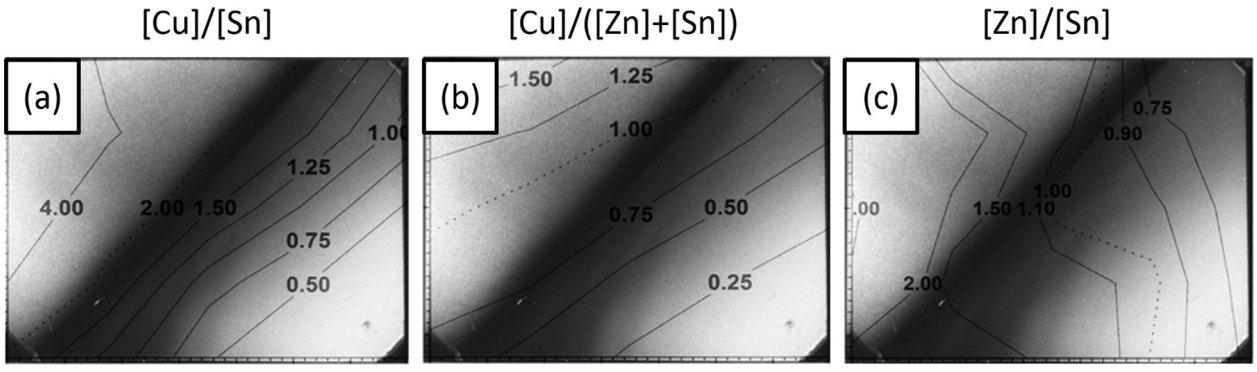

FIG. 2. Diffuse light reflection images overlaid with a compositional contour map determined by XRF. Image (a) shows that there is a clear correlation between the specular region and compositions defined by [Cu]/[Sn] ≅ 2.

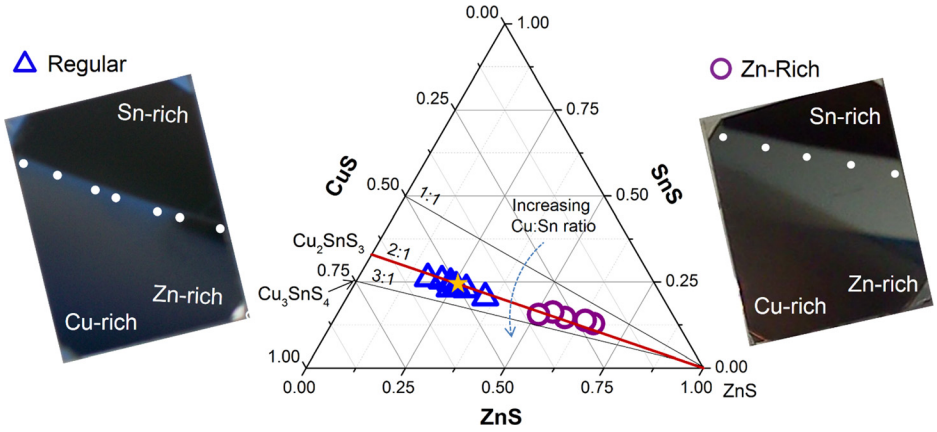

FIG. 3. Optical images of typical and Zn-rich combinatorial films are shown to the left and right of the pseudo-ternary diagram (respectively). The white spots on the sample correspond to the compositional points plotted on the diagram as blue triangles (regular) and purple circles (Zn-rich). The yellow star marks the metals composition of stoichiometric CZTS. Lines depicting [Cu]/[Sn] = 1:1, 2:1, and 3:1 are labeled as well to show that an increasing ratio moves in an arc on the diagram. The [Cu]/[Sn] = 2:1 isopleth is the CTS-CZTS-ZnS tie line and is shown in red.

or the Cu_2S-ZnS-SnS_2 pseudo-ternary diagram investigated by Olekseyuk *et al.*[4] The latter pseudo-ternary phase diagram is the one typically referenced when discussing CZTS phase equilibria, and it is from samples reacted at 1170–1420 K in a sealed glass ampoule followed by annealing at 670 K. Figure 4 displays these two possible pseudo-ternary diagrams as striped yellow and solid purple planes within the quaternary Cu-Zn-Sn-S phase diagram. They intersect along the ZnS-Cu_2ZnSnS_4-Cu_2SnS_3 tie line. The CuS-ZnS-SnS plane maintains a constant metal:S ratio, while the Cu_2S-ZnS-SnS_2 plane maintains the formal oxidation states of the metals in the kesterite structure.

For deposition conditions such as the non-equilibrium thin film route discussed herein, the phase compositions that occur do not fall on exclusively one of these planes due to combined effects of temperature, growth rate, and sulfur activity during deposition. From the phases we observe, for sufficiently high S chemical activity (recall a cracked sulfur flux is used), the ZnS-SnS_2-Cu_2SnS_3 and ZnS-CuS-Cu_2SnS_3 half planes predict the dominant observed phases for Sn- and Cu-rich compositions, respectively. The Cu_2S-ZnS-SnS_2 pseudo-ternary phase diagram, typically referenced when discussing CZTS phase equilibria, is appropriate for synthesis routes based on fixed compositions (e.g., reactants in quartz ampoules). We chose to use the CuS-ZnS-SnS phase diagram in Fig. 3 because we have observed phases such as CuS and Cu_3SnS_4 at co-deposition substrate temperature of 325 °C. However, Cu_2S and SnS_2 secondary phases lying on the Cu_2S-ZnS-SnS_2 plane were also observed in this work, and therefore only a quaternary phase diagram or a non-coplanar pseudo ternary diagram can truly reflect the phase possibilities that can occur during CZTS processing governed by unconstrained reactant amounts.

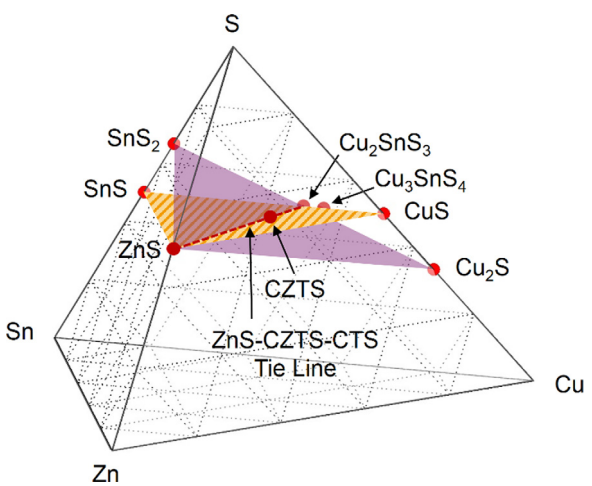

FIG. 4. CZTS quaternary phase diagram including the known phases. Two pseudo-ternary planes each containing CZTS are plotted as intersecting striped yellow and solid purple planes. The planes intersect along the ZnS-Cu_2ZnSnS_4-Cu_2SnS_3 tie line, which is shown in dashed red.

3. Coexistence of phases

Raman spectroscopy x-y mapping in part 1 (Ref. 21) showed Cu_xS phases in the Cu-rich region, SnS_2 phases in the Sn-rich region, and CZTS more concentrated closer to the specular band. Here in part 2, we extend the Raman analysis to investigate the effect of composition on the structurally coherent CZTS and CTS phases in the films deposited at 325 °C. Raman spectra were collected only from the underlying dense film even in the rough Cu- and Sn-rich regions where spectra were collected from areas between surface crystallites. ZnS also co-exists in the dense underlying film, but the excitation wavelength used in this study cannot differentiate ZnS from the structurally similar CTS and CZTS. Therefore, we do not directly analyze the ZnS content or distribution. The film shifts from Cu-rich (Cu/Sn > 2) to Sn-rich (Cu/Sn < 2) transverse to the specular band, while relative Zn-poorness to Zn-richness varies along the specular band. We analyze how these two compositional shifts alter the distribution of structurally coherent phases that comprise the dense CZTS film.

To examine the Cu-rich to Sn-rich regime, Raman spectra (Fig. 5) were collected in four spots A-D (Fig. 1), which lie on a line perpendicular to and near the middle of the specular band of the "regular" combi-CZTS sample, where Zn/(Cu + Zn + Sn) = 0.25, the stoichiometric ratio for CZTS. Both CTS and CZTS are present in all four spectra as indicated by the shoulders at 300 cm^{-1} (CTS) and 370 cm^{-1} (CZTS). The peak at 336.5 cm^{-1} appears most intense in the Sn-rich area, spot D. Tet-CTS and CZTS have nearly identical Raman-active modes (336 cm^{-1} and 337–339 cm^{-1}), so the high peak intensity could arise from higher crystalline quality CZTS within the Sn-rich region. However, we attribute this instead to a high fraction of tet-CTS coexisting with

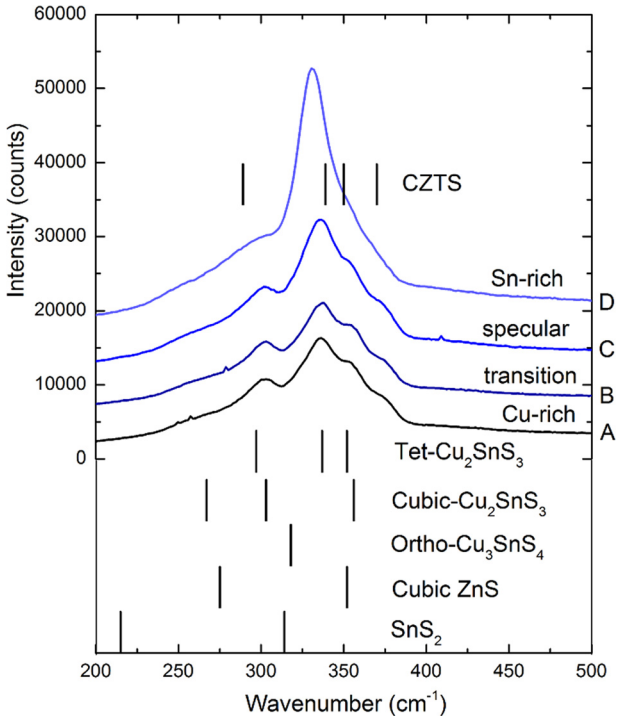

FIG. 5. Raman spectra of sample spots perpendicular to the specular band on the combi-CZTS sample. All expected peak positions are referenced from Fernandes *et al.*[20] Spot locations A-D on the sample are shown in Fig. 2.

CZTS since another tet-CTS Raman mode at 297 cm^{-1} (Ref. 20) is evident and especially broad in the spectrum of the Sn-rich area. Furthermore, the CZTS crystalline quality is expected to be poorer with increased Sn excess,[22] which is confirmed by SEM of the Sn-rich region of a similar sample in part 1 (Ref. 21) showing a porous grain structure within the main absorber layer.

The spectrum of the Sn-rich spot D does not show a resolvable local maximum for the Raman mode of SnS_2 at 318 cm^{-1}, which confirms earlier SEM observations that the structurally dissimilar SnS_2 exists only as a surface phase. Therefore, we conclude that in the Sn-rich region of this sample, tet-CTS co-exists with CZTS and SnS_2 exists only as a surface phase.

In the Cu-rich region (Fig. 5, spot A), more cub-CTS rather than tet-CTS is evident. The cub-CTS peaks at 355 and 303 cm^{-1} are more resolved and higher in intensity relative to the CZTS peaks at 336.5 and 370 cm^{-1}. Raman peaks from Cu_2S and CuS surface phases (expected at 472–475 cm^{-1} (Refs. 20 and 23)) do not appear in the spectrum from the Cu-rich region (Fig. 5, spot A), again confirming phase separation between Cu_xS and CZTS. In addition to the differences in surface phases, the major difference in the Cu- and Sn-rich regions of the sample is the cation ordering of the CTS in the dense absorber layer. Although both cubic and tetragonal phases are structurally coherent with CZTS, Sn-rich compositions favor formation of tet-CTS, while Cu-rich compositions favor more cub-CTS.

A compositionally graded Cu-Sn-S thin film was also grown at 325 °C but without Zn flux to obtain the sample shown in Fig. 6. Peaks from Raman modes of monoclinic-, cub-, and tet-CTS (Cu_2SnS_3) and orthorhombic-Cu_3SnS_4 (ortho-Cu_3SnS_4) are all observed in the spectra of the sample (Fig. 6). Spots 1–3 of the Cu-Sn-S sample follow the general trend of the Zn-containing films, where cub-CTS is favored in the Cu-rich region (Fig. 6, spot 1), and more tet-CTS is formed in the Sn-rich region (Fig. 6, spot 3), but cub-CTS is still dominant in both composition extremes. Spectra of spots 1 and 3 show evidence of both cubic and tetragonal CTS, indicating they coexist under these growth conditions.

Increasing the Cu concentration even more (Fig. 6, spot 4) results in a menagerie of phases including monoclinic-, cub-, and tet-CTS as well as orthorhombic-Cu_3SnS_4. Although cub- and tet-CTS are structurally coherent, monoclinic-CTS and orthorhombic-Cu_3SnS_4 are not.[24–26] This indicates in the initial Cu-rich growth regime at low growth temperatures, compositions of $2 < \mathrm{Cu/Sn} < 3$ are more likely to lead to cub- and tet-CTS, which are structurally coherent with CZTS. Gaussian peak fitting of the spectrum from spot 4 (which had the most well-defined peak structures) was attempted, but the resolution of the peak structure is insufficient to warrant fitting with peaks from three separate phases. Thus, the data sets from other analysis spots were also not fitted.

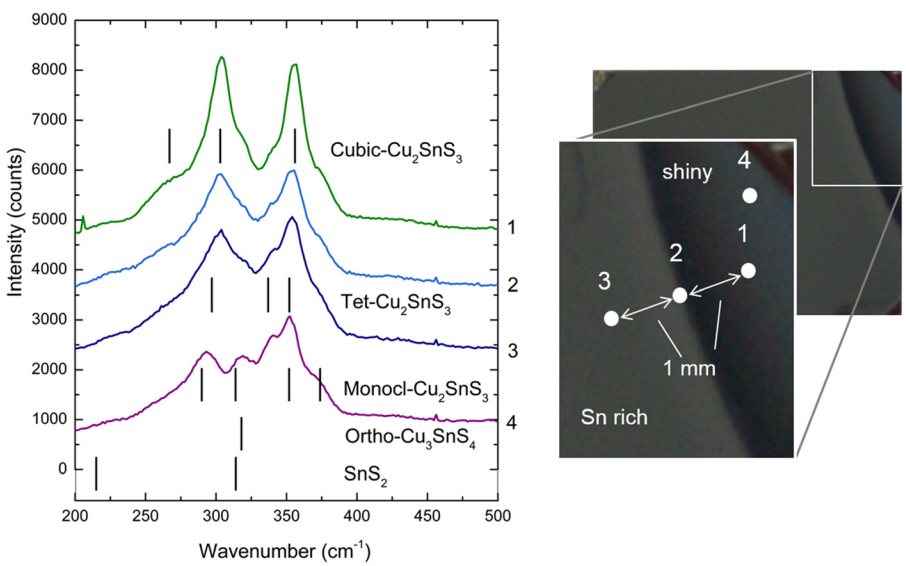

FIG. 6. Raman spectra and optical images of a Cu-Sn-S sample grown under similar conditions as the combi-CZTS samples except without Zn flux. Four distinct phases cubic- and tetragonal-Cu_2SnS_3, monoclinic-Cu_2SnS_3,[24] and orthorhombic-Cu_3SnS_4 are all observed in the Raman spectra. No peak for Cu_2S at 475 cm^{-1} or SnS peaks (below 200 cm^{-1}) are evident in the spectra.

To investigate the effect of Zn on the structurally coherent phases that co-exist with CZTS, Raman spectra of spots 1–9 (Fig. 7) were collected along the specular band, 20 μm from the abrupt transition edge to the Sn-rich region. This series of points thus maintains the constraint Cu/Sn $\sim$ 2, while only the Zn concentration varies. The shoulder at 370 cm^{-1} present in all the spectra of spots 1–9 indicates CZTS presence across the entire specular band. The "CTS shoulder" at $\sim$300 cm^{-1} also exists in all the spectra from the specular band, even in the Zn-rich region.

As the film becomes more Zn-poor, the tet-CTS phase is favored over cub-CTS. The CTS shoulder progressively broadens from the Zn-poor spot 1 spectrum to the Zn-rich spot 9 spectrum. This indicates the increasing fraction of tet-CTS within the coherent CTS/CZTS film. Additionally, the peak intensities of the 303 and 356 cm^{-1} Raman modes of cub-CTS relative to the dominant peak at 336.5 cm^{-1}, common to both CZTS and tet-CTS, are higher in the spectrum of the Zn-poor region (Fig. 7, spot 1). Both the broadening of the CTS shoulder with increased Zn content and the increase in cub-CTS modes in the Zn-poor region indicate a higher cub-CTS fraction in the Zn-poor region of the specular band. Although these data show trends for cub- or tet-CTS preference in either Zn-poor or Zn-rich conditions (respectively), both crystalline structures still co-exist even at the extremes analyzed. Figure 8 displays the clear co-existence of tet-CTS, cub-CTS, and CZTS in the Zn-poor region of the film near spot 1.

Since the CTS shoulder persists in the "regular" sample, a Zn-rich sample grown under similar conditions but with a higher Zn flux was also examined by Raman spectroscopy to determine if raising the Zn fraction in the film would decrease the fraction of CTS. The composition along this "Zn-rich" sample's specular band (Fig. 3) also lies on the ZnS-CZTS-CTS tie line on the CZTS pseudo-ternary phase diagram but with higher Zn fractions than the "regular" sample. Figure 9 compares the Raman spectra of the two samples and demonstrates that despite the Zn-rich composition lying clearly in the region of the pseudo-ternary diagram where CTS is not stoichiometrically favored, the CTS shoulder still persists.

Raman analyses of metal stacks sulfurized at 400 °C also showed CTS presence in samples with stoichiometric CZTS composition.[18] These and our findings differ from Olekseyuk's phase diagram,[4] which indicates CZTS is the thermodynamically stable phase at the stoichiometric CZTS composition on the 670 K ($\sim$400 °C) isotherm. The persistence of CTS despite adequate Zn indicates these thin films have not reached thermodynamic equilibrium at growth temperatures of 325 °C. Because the CTS phase changes with Sn, Cu, and Zn chemical potential across the film, we can observe the changes in composition-dependent cation arrangement by examining the changes in cub- and tet-CTS across these compositionally graded thin films grown at low temperature.

Figure 10 depicts the trend of more cub-CTS bonding characteristics in Cu-rich and Zn-poor regions of the sample

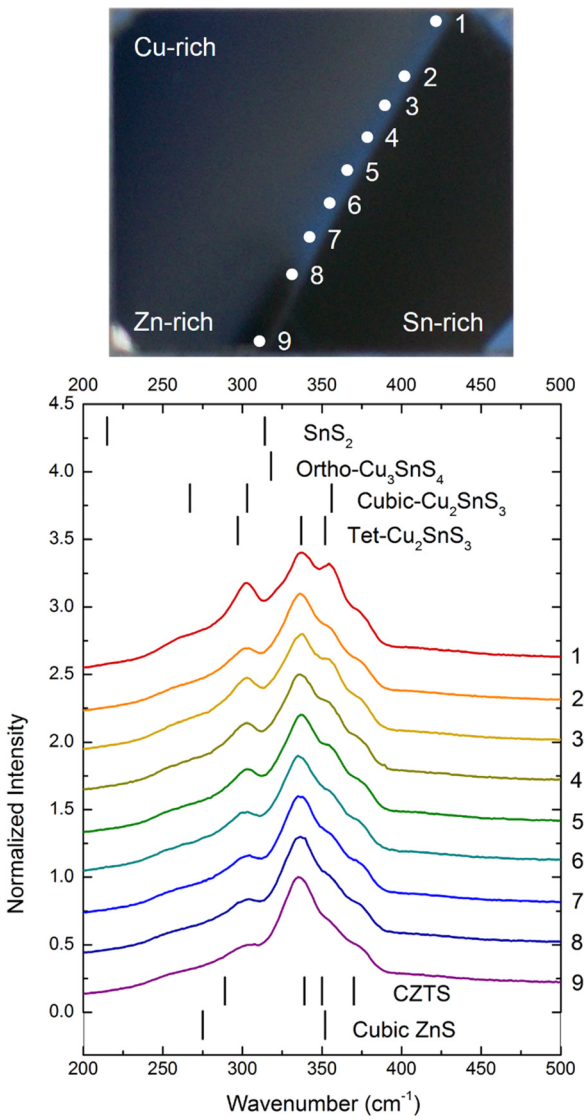

FIG. 7. Raman spectra for spots along the specular band of the regular combinatorial CZTS sample. Reference peak positions expected for CZTS and commonly expected secondary phases are shown below the spectra.[20]

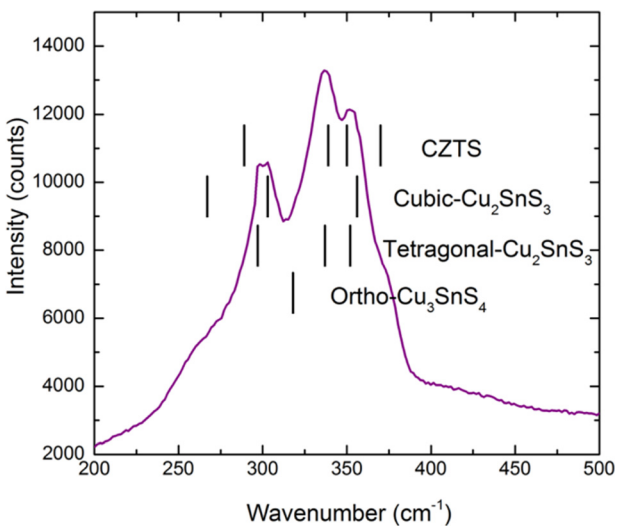

FIG. 8. Co-existence of tet- and cub-CTS phases is clearly discernible in the Raman spectrum collected on the rough side of the specular/rough edge near spot 1 (identified in Fig. 7).

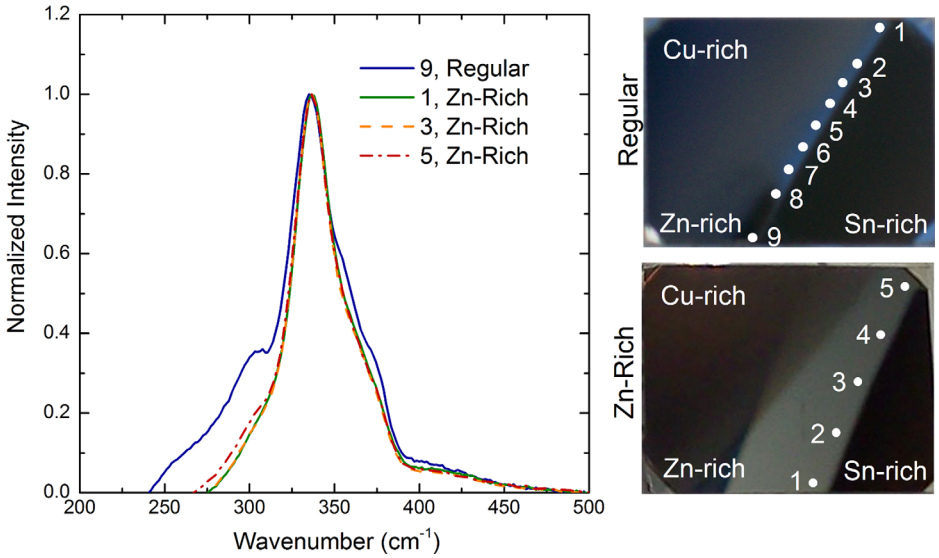

FIG. 9. Raman spectra from the Zn-rich area on the "regular" combi-CZTS sample and from the "Zn-rich" combi-CZTS sample. The spectra are normalized after a linear background subtraction.

grown at 325 °C and more tet-CTS bonding characteristics in Sn- and Zn-rich regions. Note that no region contains exclusively cub- or tet-CTS. Two unit cells of cub-CTS have the same lattice parameters as one unit cell of tet-CTS (a = 5.434 Å for cub-CTS and a = b = 5.412, c = 10.810 Å for tet-CTS (Ref. 25)), so the difference between these phases is not the lattice structure but rather the Cu and Sn cation site occupations. The metals are randomly distributed in cub-CTS, whereas the Cu and Sn site occupation within tet-CTS is more ordered (Figs. 11(a) and 11(b)).

For tet-CTS, the 2a Wyckoff cation sites with coordinates (0,0,0) are occupied only by Cu, leaving the remaining 4d and 2b cation sites with coordinates of $(0,\frac{1}{2},\frac{1}{4})$ and $(0,0,\frac{1}{2})$ having observed 44% or 46% probability of Sn occupation[28] (Fig. 11(b)). In cub-CTS, random distribution results in only 33% probability that Sn will occupy *any* cation site in the lattice (Fig. 11(a)). When comparing these site occupation probabilities with kesterite and stannite CZTS (Figs. 11(c) and 11(d)) and considering that Zn can more easily displace Cu than Sn,[29] it is evident that tet-CTS has a higher probability for 2a and 2b sites having the same metal occupation as kesterite or stannite CZTS. However, cub-CTS has a higher probability that 4d sites will have the same metal occupation as kesterite or stannite CZTS assuming facile Cu/Zn exchange. Since a clear conclusion such as "the probability of Cu and Sn arrangement in tet-CTS is more like kesterite (or stannite) CZTS than for cub-CTS" cannot be drawn, thinking of cation arrangement in a different way may be more helpful.

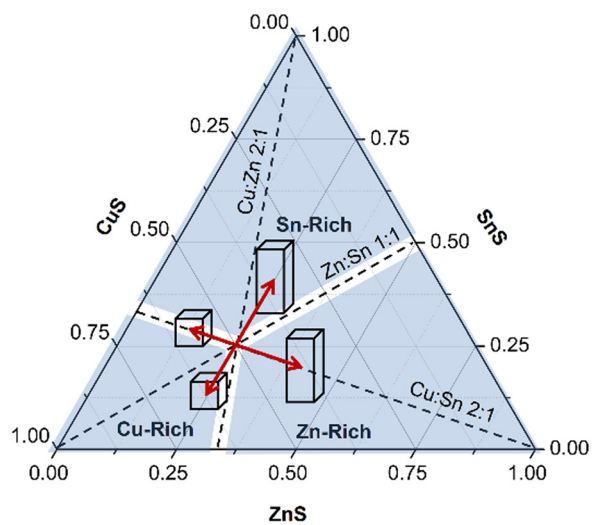

FIG. 10. The Cu/Sn = 2, Cu/Zn = 2, and Zn/Sn = 1 tie lines, which determine the boundaries for Cu-, Sn-, and Zn-rich regions on the pseudo-ternary diagram are all drawn, and each zone is labeled. Cu-rich conditions are Cu/Sn > 2 and Cu/Zn > 2. Sn-rich conditions are Cu/Sn < 2 and Zn/Sn < 1. Zn-rich conditions are Cu/Sn < 2 and Zn/Sn > 1. The trends in crystalline structures of the Cu_2SnS_3, which co-exists with CZTS and ZnS within these different compositional regions on films grown at 325 °C, are depicted by either a cube (cubic-Cu_2SnS_3) or a cuboid (tetragonal-Cu_2SnS_3).

Zhai *et al.*[13] emphasize differences in cation arrangement can also be viewed as differences in tetrahedral coordination of the metallic cations to the sulfur atom within the CTS lattice. The most stable CTS structures are predicted to be a combination of Cu_3Sn and Cu_2Sn_2 coordination to the S atoms.[13] For the Cu-Sn-S system, a Cu_3Sn tetrahedral coordination (Fig. 11(e)) is most analogous to kesterite and stannite CZTS, which both have Cu_2ZnSn tetrahedral coordination for S atoms. Although differences between tet- or cub-CTS can be discussed as differences of Cu or Sn occupation on specific sites or differences in the tetrahedral coordination to the S atom, the main point is the cation arrangement within CTS phase changes with composition. At typical growth temperatures for CZTSe coevaporation, CTSe is not observed, and CZTSe forms from Cu_xSe, ZnSe, and SnSe,[17] so we also examined a film grown at 470 °C to determine how composition variation affected CZTS.

B. High temperature film deposited at 470 °C

1. Surface morphology and composition

Part 1 (Ref. 21) of this study showed that the major morphological difference between the samples grown at 325 °C and 450 °C was the conversion of the entire Sn-rich (Cu/Sn < 2) rough region into a specularly reflective film. The higher growth temperature allowed for self-limiting

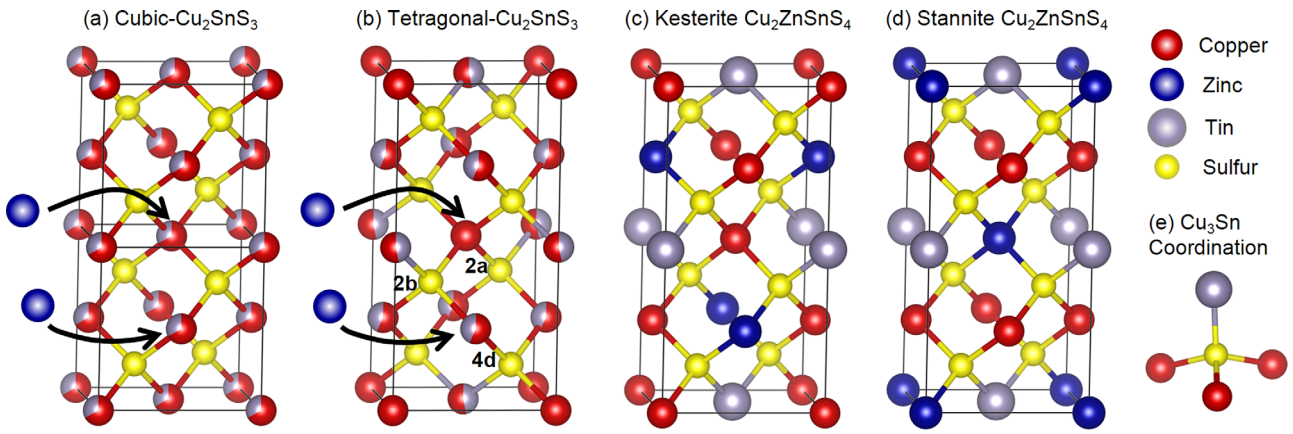

FIG. 11. (a) Two unit cells of cubic-Cu_2SnS_3, (b) tetragonal-Cu_2SnS_3,[27] (c) kesterite, and (d) stannite Cu_2ZnSnS_4.[28] Both cub- and tet-CTS have the same cation sites, but the probability of Cu (red) or Sn (gray) occupation differs and is represented by partial coloring of each atom. Zn (blue) substitution on the 2a and 4d sites of tet-CTS and the analogous sites in the cub-CTS are represented and emphasizes the difference in Zn displacing Cu vs. Sn to form kesterite or stannite CZTS. (e) Cu_3Sn tetrahedral coordination to S (yellow).

incorporation of SnS;[14,15,17] therefore, the compositions of the regions under excess Sn flux collapsed to the CZTS-CTS-ZnS tie line and thus were specularly reflective because they lacked Sn_xS_y surface phases. The sample examined in this second part of the study was grown at 470 °C. It would otherwise be specularly reflective like the samples grown at 450 °C in part 1, except excess Sn and S fluxes were used during cooling in an attempt to prevent CZTS decomposition. As a result, Sn_xS_y phases, which appear as faceted and flake-like grains in SEM, are present on the surface of the entire sample. There is no obvious specular band on this sample but specular reflectivity is observed when viewed at glancing angles. Figure 12(a) displays the composition range of this sample on the pseudo-ternary phase diagram. As is expected for Sn-rich samples at high growth temperatures, the composition lies nearly on the CTS-CZTS-ZnS tie line. Figure 12(b) displays the corresponding Raman spectra of the sample's four corners and the center.

2. Coexistence of phases

Although the surface morphology and film porosity improves for Sn-rich regions at higher growth temperatures in part 1, the PL studies showed a dramatic drop in intensity from the regions with Cu-rich to Sn-rich fluxes. This likely resulted from deleterious Sn-related native point defects. In the Cu-rich regions (Cu/Sn > 2) of these same films, however, the PL intensity increased as the Zn concentration of

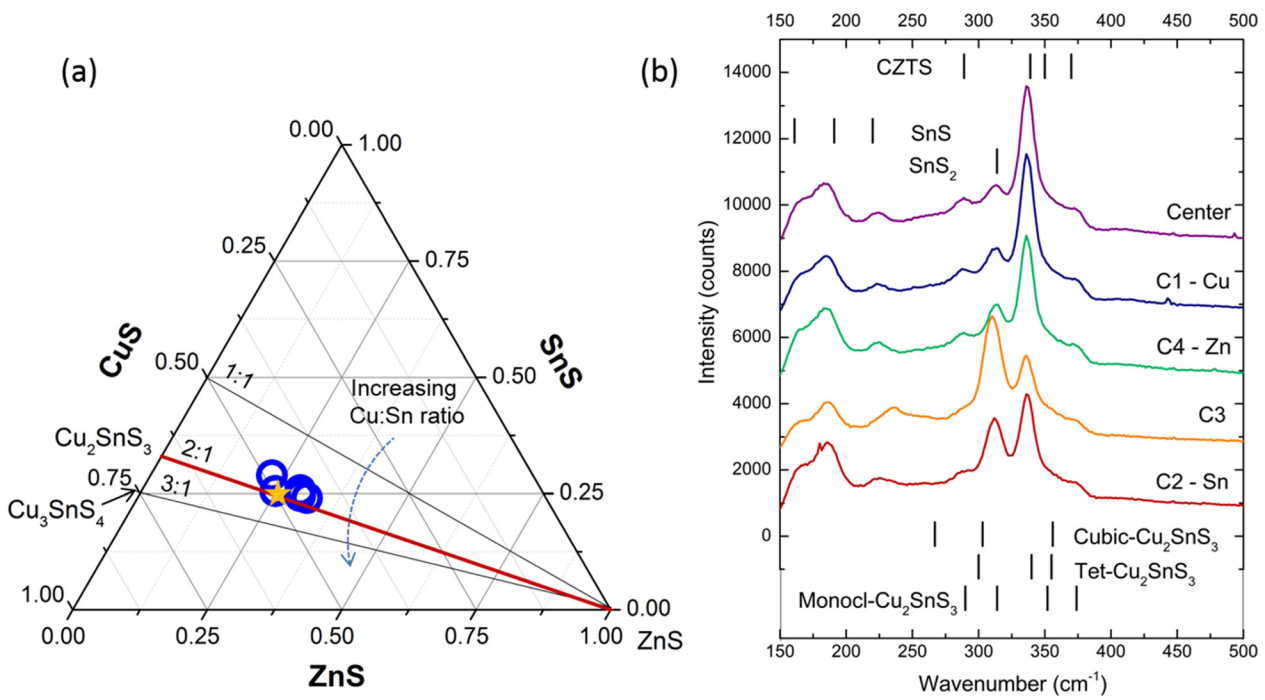

FIG. 12. The compositions of the middle and four corners of a thin film of CZTS deposited at 470 °C are plotted on the pseudo-ternary diagram (a). The Raman spectra of five spots, the center and C1-C4 (corners 1–4), are plotted on the graph in (b). Reference peak positions[20] expected for CZTS and commonly expected secondary phases are shown on the Raman plots.

the film increased. This second portion of the study uses Raman spectroscopy to further investigate the effect of composition variation during higher growth temperatures. Only CZTS (no CTS) was present, and the overall CZTS crystalline quality increased compared to the 325 °C samples. We also found that excess Sn flux during growth induced more crystalline disorder (variation in metal-sulfur vibrational mode energy) in CZTS; however, the crystalline quality is relatively insensitive to excess Zn.

The Raman spectra of the 4 corners and the center of the sample deposited at 470 °C (Fig. 12(b)) indicate that CZTS is present across the entire film. The characteristic CTS shoulder at 300 cm^{-1} prevalent in the samples deposited at 325 °C does not appear in these spectra and indicates the lack of CTS at this higher growth temperature. Note again that ZnS may be present in these composition extremes; however, it is difficult to differentiate from CZTS via Raman using a visible laser. Unlike the samples deposited at 450 °C in part 1 of this study, Sn_xS_y phases are observed over the entire sample surface due to the Sn flux exceeding the Sn/SnS vapor pressure during cooling from the growth temperature to prevent CZTS decomposition. The Sn_xS_y peaks in the spectra are not a direct result of increased growth temperature, and are not expected to change the overall trends for CZTS crystalline quality discussed later since they occur post-deposition as surface phases. However, we discuss them to show the possible phases that may occur under such post-deposition conditions and emphasize there is no major overlap between CZTS and Sn_xS_y Raman active modes.

Peaks at 166, 184, and 223 cm^{-1} (Fig. 12(b)) indicate SnS presence on the surface of the film. The observed peaks differ from previously reported results[20] for SnS at 160, 190, and 219 cm^{-1}. However, the 2_{Ag} mode was observed[20,30,31] in the range of 219–223 cm^{-1}, and the B_{2g} mode, which is the most intense peak observed by us and Fernandes *et al.*,[20] is observed as low as 182 cm^{-1} in SnS nanoparticles.[32] A peak shift may occur with variation in the Sn-S coordination in the Sn_xS_y phases, where x and y are not integers. The peak at 314 cm^{-1}, in the spectra of three of the four corners and the center of the sample (Fig. 12(b), center, Zn, Cu, and Sn) corresponds to SnS_2.[20] The spectrum from the corner with more sulfur relative to the metals' compositional fraction has Raman modes at 310 and 235 cm^{-1}, which correspond more closely to previously reported[33] Sn_2S_3 Raman active modes (307 and 234 cm^{-1}) rather than those of SnS or SnS_2.

The main differences between the combi-CZTS films deposited at 325 °C and 470 °C as seen in the Raman spectra (Fig. 13) are the disappearance of the CTS phase and the increased crystalline quality of the CZTS. Figure 13 directly compares Raman spectra from combinatorial CZTS grown at 325 and 470 °C. The low temperature spectrum (dashed line) was collected from spot 9 on the "regular CZTS" sample grown at 325 °C (Fig. 7), and the spectrum for the high temperature sample (solid line) was collected from the center of the high temperature film (Fig. 12(b), center). The FWHM (full width at half maximum) of the main CZTS peak at 336.5 cm^{-1} decreased from 25 cm^{-1} to 15 cm^{-1} as the growth temperature was increased from 325 to 470 °C. This

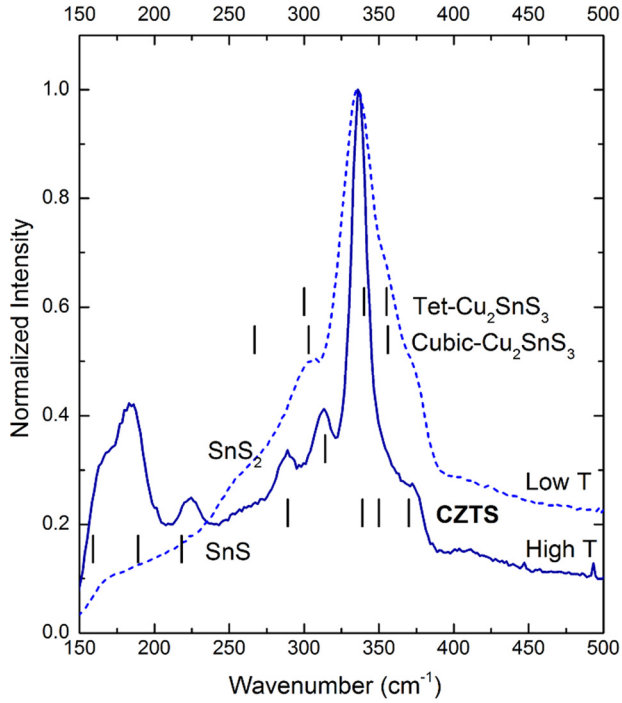

FIG. 13. Raman spectra of films deposited at 325 °C (low T, dotted line) and at 470 °C (high T, solid line) are compared with background subtraction and normalization. The narrower CZTS peak at 336.5 cm^{-1} for the high temperature sample indicates higher crystalline perfection.

decrease in CZTS peak width indicates longer phonon mean free path and thus a higher degree of crystalline order.

In addition to increased deposition temperature, a Cu-rich (Cu/Sn > 2) composition also results in more ordered CZTS. Raman spectra from corner 3 (Cu/Sn = 1.7) and the center (Cu/Sn = 1.9) are selected to compare, since these points both maintain constant Cu/Zn = 1.5, and lie within the desired final Cu-poor, Zn-rich regime. The FWHM of the main CZTS peak at 336.5 cm^{-1} increases almost 50% from 15 to 22 cm^{-1} with only 4% increase in the Cu/(Cu + Sn) ratio. The peak at 336.5 cm^{-1} arises from the A mode in CZTS and is attributed only to anion motion.[34] Since sulfur is coordinated to all metals in CZTS, this FWHM analysis is sensitive to crystalline disorder that may result from cation substitution or vacancies of any of the three metals. The trend of decreasing crystalline quality with increased Sn flux during film growth is also evident when comparing corners 1 (Cu) and 2 (Sn), where the FWHM increases from 15 to 18 cm^{-1} for regions under high Cu vs. high Sn fluxes. The observation of lower crystalline order with higher Sn flux despite the self-limiting nature of SnS and improved morphology at a higher growth temperature agrees with the attribution of low PL response observed in part 1 to higher concentrations of Sn-related native defects.

Conversely, a Zn-rich (Cu/Zn < 2) flux during growth at 470 °C does not significantly impact the crystalline quality of the CZTS within the Cu-rich region. The Raman spectra from corners 4 (Cu/Zn = 1.9) and 1 (Cu/Zn = 1.4) (Fig. 12(b), 4-Cu and 1-Zn) are selected to compare, since these points both maintain a constant Cu/Sn = 1.8. An 18% mole fraction increase in Zn/(Cu + Zn) from corner 4 to corner 1 does not change the 15 cm^{-1} FWHM of the main CZTS peak at 336.5 cm^{-1}. Both

spectra show the same FWHM as well as relatively similar peak intensities. This insensitivity of the FWHM of the CZTS peak to the Zn content in the final film indicates that excess Zn does not induce significant variation in the metal-sulfur bonds from native antisite defects within the CZTS grains to the same extent as the disruptive effects of excess Sn.

Two stage coevaporation of CZTSe[6,17] harnesses the benefits of both initial Cu-rich growth (Cu/(Zn + Sn) > 1) for larger grains, and final Zn-rich growth that results in the Cu-poor, Zn-rich composition near the buffer layer interface common to all high efficiency CZTSSe devices. Sn incorporation into CZTS(Se) has been assumed to be self-limiting during growth with sufficiently high Sn and S(Se) vapor pressures. Part 1 shows a dramatic drop in PL intensity related to excess Sn flux on samples grown at 450 °C even though the final CZTS composition remains stoichiometric. In films grown at 325 °C which are kinetically trapped, we observed a change in Cu and Sn arrangement, evident by the shift in the CTS secondary phase from more cub-CTS in the Cu-rich region (Cu/Sn > 2) to more tet-CTS in Sn-rich region (Cu/Sn < 2). For CZTS samples grown at 470 °C (similar to those in part 1), the volatile CTS is not present, and regions grown under excess Sn flux are more disordered than Cu-rich regions, evident by an increased FWHM in the peak for the Raman active A mode of CZTS. Therefore, increasing Sn chemical potential changes cation arrangement in CTS and results in more CZTS lattice disorder. These findings suggest that high Sn chemical potential adversely changes the cation arrangement within CZTS. However, experiments that directly measure the change in cation ordering in CZTS with variance in Sn chemical potential are necessary to validate this theory.

During the initial Cu-rich growth of CZTSe during 2-stage coevaporation, Cu_xS phases may induce larger grain growth[6] by precipitating dendritic structures of the precursor CTS (or CZTS) within the Cu_xS matrix, similar to the effects[35] of growing $CuInSe_2$ in the presence of Cu_xSe which promotes fluxing and increased lateral grain growth. Mousel *et al.*[19] also showed that precursors grown in Cu-rich conditions led to higher device efficiencies after the Cu_xSe phases were etched out of Cu-Zn-Sn-Se precursors before selenization, leaving the final CZTS film composition Cu-poor. This highlights that the benefits of initial Cu-rich growth extend beyond the fluxing assistance from $Cu_xS(Se)$. We postulate initial Cu-rich (Cu/Sn > 2) CZTS growth results in a more ordered CZTS lattice due to favorable tetrahedral Cu_3Sn or Cu_2ZnSn coordination to the S atom, whereas Sn-rich growth may favor multiple Sn atoms coordinated to one S atom. The antisite defect formation energies predicted by Chen *et al.*[29] indicate relatively low energies for Cu/Zn exchanges, higher energies for Sn/Zn exchange, and the highest energies for Sn/Cu exchange. Therefore, growth with Cu/Sn > 2 may secure Sn site occupancy with low Sn antisite defects. When more Zn is introduced later during coevaporation, the Zn atoms are more likely to displace a Cu atom as opposed to a Sn atom. We finally propose that finely controlling the Sn chemical potential within Cu-rich growth environment may establish preferred Cu_3Sn or Cu_2ZnSn coordination to the S atom and lead to fewer Sn antisite defects in CZTS. This is to say that simply supplying a large SnS(Se) overpressure may be sufficient to prevent CZTS decomposition; however, this strategy will guarantee the presence of minority carrier lifetime-killing deep states and thus the degree of SnS excess must be carefully tuned. Furthermore, the Zn_{Sn} antisite defect may be relatively benign, whereas the Cu_{Sn} or V_{Sn} defects are deeper within the bangap.[29] Thus, excess Zn may benefit a slight Sn deficiency without deleterious effects to overall CZTS lattice disorder. This is in agreement with part 1 (Ref. 21) that shows increased PL intensity with increased Zn fraction within the Cu/Sn > 2 region of the films grown at 450 °C.

IV. CONCLUSIONS

Morphological studies of compositionally graded CZTS thin films grown at 325 °C reveal a specular band with composition lying on the ZnS-CZTS-CTS tie line on the pseudo-ternary phase diagram containing CZTS.[21] In the low temperature combi-CZTS films, observed surface phases of CuS and SnS_2 did not appear in the Raman spectra of the underlying dense CZTS layer, indicating that only structurally coherent phases (cub- and tet-CTS and ZnS) are incorporated in the CZTS film, and all structurally incoherent secondary phases (CuS, SnS_2) are embedded as separate grains or exist only as surface phases. Determination of secondary phases using Raman spectroscopy shows a CTS phase across the entire sample, even in Zn-rich regions. The more disordered cub-CTS intermediate forms preferentially to the more ordered tet-CTS in Cu-rich and Zn-poor compositions, which are the initial growth conditions in 2 stage coevaporation, which lead to better grain growth and ultimately higher device efficiencies. The shift from tetragonal to cubic-CTS phase indicates a change in Cu and Sn cation order with a shift in composition. A higher growth temperature of 470 °C results in CZTS with no CTS, and better crystalline quality is obtained in the Cu-rich regions of the films. The Zn fraction has no measurable effect on crystalline quality at these higher growth temperatures. Considering both the low and high temperature growth results, we propose the observed higher crystalline quality in initial Cu-rich, Zn-poor growth of CZTS is related to the cation site occupations within the zinc-blende lattice, common to ZnS, CTS, and CZTS, which can be manipulated with composition. Initial Cu-rich growth during 2-stage coevaporation of CZTS may form more favorable Cu_3Sn or Cu_2ZnSn tetrahedral coordination on the S atoms, which may lead to fewer Sn antisite defects in CZTS. A Zn-rich final film composition with Cu/Sn < 2, which is obtained during the second stage, does not deleteriously affect overall CZTS crystalline quality.

ACKNOWLEDGMENTS

The research at the University of Utah was supported in whole by the U.S. Department of Energy, Office of Basic Energy Sciences, Division of Materials Sciences and Engineering under Award No. DE-SC0001630. The work at NREL was supported by the U.S. Department of Energy under Contract No. DE-AC36-08GO28308 with the National Renewable Energy Laboratory.

[1]W. Wang, M. T. Winkler, O. Gunawan, T. Gokmen, T. K. Todorov, Y. Zhu, and D. B. Mitzi, Adv. Energy Mater. (published online).
[2]T. K. Todorov, J. Tang, S. Bag, O. Gunawan, T. Gokmen, Y. Zhu, and D. B. Mitzi, Adv. Energy Mater. **3**, 34 (2013).
[3]B. Shin, O. Gunawan, Y. Zhu, N. A. Bojarczuk, S. J. Chey, and S. Guha, Prog. Photovoltaics **21**, 72 (2013).
[4]I. Olekseyuk, I. V. Dudchak, and L. V. Piskach, J. Alloys Compd. **368**, 135 (2004).
[5]S. Chen, X. G. Gong, A. Walsh, and S. Wei, Appl. Phys. Lett. **96**, 021902 (2010).
[6]I. Repins, C. Beall, N. Vora, C. DeHart, D. Kuciauskas, P. Dippo, B. To, J. Mann, W.-C. Hsu, A. Goodrich, and R. Noufi, Sol. Energy Mater. Sol. Cells **101**, 154 (2012).
[7]K. Wang, B. Shin, K. B. Reuter, T. Todorov, D. B. Mitzi, and S. Guha, Appl. Phys. Lett. **98**, 051912 (2011).
[8]J. Timo Waütjen, J. Engman, M. Edoff, and C. Platzer-Bjoürkman, Appl. Phys. Lett. **100**, 173510 (2012).
[9]J. Just, D. Luützenkirchen-Hecht, R. Frahm, S. Schorr, and T. Unold, Appl. Phys. Lett. **99**, 262105 (2011).
[10]A. Fairbrother, E. García-Hemme, V. Izquierdo-Roca, X. Fontané, F. A. Pulgarín-Agudelo, O. Vigil-Galán, A. Pérez-Rodríguez, and E. Saucedo, J. Am. Chem. Soc. **134**, 8018 (2012).
[11]A. Walsh, S. Chen, X. G. Gong, S.-H. Wei, J. Ihm, and H. Cheong, AIP Conf. Proc. 63–64 (2011).
[12]B. G. Mendis, M. C. J. Goodman, J. D. Major, A. A. Taylor, K. Durose, and D. P. Halliday, J. Appl. Phys. **112**, 124508 (2012).
[13]Y.-T. Zhai, S. Chen, J.-H. Yang, H.-J. Xiang, X.-G. Gong, A. Walsh, J. Kang, and S.-H. Wei, Phys. Rev. B **84**, 075213 (2011).
[14]A. Weber, R. Mainz, and H. W. Schock, J. Appl. Phys. **107**, 013516 (2010).
[15]J. J. Scragg, T. Ericson, T. Kubart, M. Edoff, C. Platzer-Björkman, and C. Platzer-bj, Chem. Mater. **23**, 4625 (2011).
[16]A. Redinger, D. M. Berg, P. J. Dale, and S. Siebentritt, J. Am. Chem. Soc. **133**, 3320 (2011).
[17]G. Kaune, S. Hartnauer, F. Syrowatka, and R. Scheer, Sol. Energy Mater. Sol. Cells **120**, 596 (2014).
[18]A.-J. Cheng, M. Manno, A. Khare, C. Leighton, S. A. Campbell, and E. S. Aydil, J. Vac. Sci. Technol., A **29**, 051203 (2011).
[19]M. Mousel, T. Schwarz, R. Djemour, T. P. Weiss, J. Sendler, J. C. Malaquias, A. Redinger, O. Cojocaru-Mirédin, P.-P. Choi, and S. Siebentritt, Adv. Energy Mater. **4**(2) (2013).
[20]P. A. Fernandes, P. M. P. Salomé, and A. F. da Cunha, J. Alloys Compd. **509**, 7600 (2011).
[21]H. Du, F. Yan, M. Young, B. To, C.-S. Jiang, P. Dippo, D. Kuciauskas, Z. Chi, E. A. Lund, C. Hancock, W. M. Hlaing OO, M. A. Scarpulla, and G. Teeter, J. Appl. Phys. **115**, 173502 (2014).
[22]J. J. Scragg, *Copper Zinc Tin Sulfide Thin Films for Photovoltaics* (Springer Berlin Heidelberg, Berlin, 2011).
[23]B. Minceva-Sukarova, M. Najdoski, I. Grozdanov, and C. J. Chunnilall, J. Mol. Struct. **410–411**, 267 (1997).
[24]D. M. Berg, R. Djemour, L. Gütay, S. Siebentritt, P. J. Dale, X. Fontane, V. Izquierdo-Roca, and A. Pérez-Rodriguez, Appl. Phys. Lett. **100**, 192103 (2012).
[25]P. A. Fernandes, P. M. P. Salomé, and A. F. da Cunha, J. Phys. D: Appl. Phys. **43**, 215403 (2010).
[26]F. Hergert and R. Hock, Thin Solid Films **515**, 5953 (2007).
[27]X. Chen, H. Wada, A. Sato, and M. Mieno, J. Solid State Chem. **139**, 144 (1998).
[28]S. Chen, X. G. Gong, A. Walsh, and S.-H. Wei, Appl. Phys. Lett. **94**, 041903 (2009).
[29]S. Chen, A. Walsh, X.-G. Gong, and S.-H. Wei, Adv. Mater. **25**, 1522 (2013).
[30]X.-L. Gou, J. Chen, and P.-W. Shen, Mater. Chem. Phys. **93**, 557 (2005).
[31]Y. Liu, D. Hou, and G. Wang, Chem. Phys. Lett. **379**, 67 (2003).
[32]S. Sohila, M. Rajalakshmi, C. Ghosh, A. K. Arora, and C. Muthamizhchelvan, J. Alloys Compd. **509**, 5843 (2011).
[33]L. S. Price, I. P. Parkin, A. M. E. Hardy, R. J. H. Clark, T. G. Hibbert, and K. C. Molloy, Chem. Mater. **11**, 1792 (1999).
[34]T. Gürel, C. Sevik, and T. Çağın, Phys. Rev. B **84**, 205201 (2011).
[35]J. S. Park, Z. Dong, S. Kim, and J. H. Perepezko, J. Appl. Phys. **87**, 3683 (2000).